J. Fluid Mech. (1990), *vol.* 212, *pp.* 337–363
Printed in Great Britain

On a class of steady confined Stokes flows with chaotic streamlines

By K. BAJER† AND H. K. MOFFATT

Department of Applied Mathematics and Theoretical Physics, University of Cambridge, Silver Street, Cambridge CB3 9EW, UK

(Received 3 May 1989)

The general incompressible flow $\boldsymbol{u}^{Q}(\boldsymbol{x})$, quadratic in the space coordinates, and satisfying the condition $\boldsymbol{u}^{Q}\cdot\boldsymbol{n}=0$ on a sphere $r=1$, is considered. It is shown that this flow may be decomposed into the sum of three ingredients – a poloidal flow of Hill's vortex structure, a quasi-rigid rotation, and a twist ingredient involving two parameters, the complete flow $\boldsymbol{u}^{Q}(\boldsymbol{x})$ then involving essentially seven independent parameters. The flow, being quadratic, is a Stokes flow in the sphere.

The streamline structure of the general flow is investigated, and the results illustrated with reference to a particular sub-family of 'stretch–twist–fold' (STF) flows that arise naturally in dynamo theory. When the flow is a small perturbation of a flow $\boldsymbol{u}_1(\boldsymbol{x})$ with closed streamlines, the particle paths are constrained near surfaces defined by an 'adiabatic invariant' associated with the perturbation field. When the flow $\boldsymbol{u}_1$ is dominated by its twist ingredient, the particles can migrate from one such surface to another, a phenomenon that is clearly evident in the computation of Poincaré sections for the STF flow, and that we describe as 'trans-adiabatic drift'. The migration occurs when the particles pass a neighbourhood of saddle points of the flow on $r=1$, and leads to chaos in the streamline pattern in much the same way as the chaos that occurs near heteroclinic orbits of low-order dynamical systems.

The flow is believed to be the first example of a steady Stokes flow in a bounded region exhibiting chaotic streamlines.

1. Introduction

Study of the kinematics of fluid flow normally begins with analysis of the velocity field $\boldsymbol{u}(\boldsymbol{x})$ in the neighbourhood of a point O (see, for example, Batchelor 1967, §2.3). Taking origin at O, the Taylor series of $u_i(\boldsymbol{x})$ has the form

$$u_i(\boldsymbol{x}) = a_i + b_{ij}x_j + c_{ijk}x_j x_k + \dots, \tag{1.1}$$

where

$$a_i = u_i(0), \quad b_{ij} = \left.\frac{\partial u_i}{\partial x_j}\right|_{x=0}, \quad c_{ijk} = \left.\frac{\partial^2 u_i}{\partial x_j \partial x_k}\right|_{x=0} = c_{ikj}, \dots. \tag{1.2}$$

Study of the linear term $b_{ij}x_j$ shows that locally the relative motion consists of three parts: spherically symmetric dilatation associated with the trace b_{ii} (zero for incompressible flow), irrotational strain associated with the symmetric part of $b_{ij}-\frac{1}{3}\delta_{ij}b_{kk}$, and quasi-rigid rotation associated with the antisymmetric part of b_{ij}.

We shall in this paper consider some effects associated with the quadratic term

† On leave of absence from the Institute of Geophysics, University of Warsaw, Poland.

$c_{ijk}x_jx_k$ in the expansion (1.1). Most important among these is that, whereas the streamlines of the linear approximation

$$u_i^{\mathrm{L}} = a_i + b_{ij}x_j \tag{1.3}$$

are in general unbounded (the only exception being when $\boldsymbol{a} = 0$ and $b_{ij} = -b_{ji}$, when they are circles), the streamlines of the quadratic approximation

$$u_i^{\mathrm{Q}} = a_i + b_{ij}x_j + c_{ijk}x_jx_k \tag{1.4}$$

may, for a wide choice of a_i, b_{ij}, c_{ijk}, be contained within a bounded region. We shall in fact find that there is, apart from an arbitrary multiplicative constant, a seven-parameter family of flows of the form (1.4) satisfying the incompressibility condition

$$\boldsymbol{\nabla}\cdot\boldsymbol{u}^{\mathrm{Q}} = 0 \tag{1.5}$$

and the condition of zero normal velocity on a sphere which we may assume to have unit radius:

$$\boldsymbol{x}\cdot\boldsymbol{u}^{\mathrm{Q}} = 0 \quad \text{on} \quad r = 1, \tag{1.6}$$

where $r^2 = \boldsymbol{x}\cdot\boldsymbol{x}$.

Boundedness of the streamlines within the sphere $r < 1$ does not of course imply that these streamlines are closed curves, nor even that they lie on a family of surfaces within the sphere. They may exhibit the phenomenon of chaotic wandering that has been found for the particle paths of certain time-periodic two-dimensional flows by Aref (1984), Aref & Balachandar (1986) and Chaiken *et al.* (1986, 1987), and for the streamlines of certain space-periodic, steady, flows (the 'ABC'-flows) by Hénon (1966) and Dombre *et al.* (1986). We shall indeed find that the general quadratic flow of the form (1.4) satisfying (1.5) and (1.6) does have chaotic streamlines in at least part of the spherical domain, with corresponding implications for the spread of any scalar field convected by such a flow, and for the spread and intensification of any vector field convected and distorted by the flow.

It was in fact in this latter context that a particular quadratic flow was devised (Moffatt & Proctor 1985) to represent the stretch–twist–fold (STF) action that is believed to be most conducive to so-called 'fast dynamo action' in magneto-hydrodynamics (see Vainshtein & Zel'dovich 1972; Zel'dovich, Ruzmaikin & Sokolov 1983, chap. 7). This flow suffered from the undesirable property of unbounded streamlines, a defect that has been remedied by Bajer (1989) by the simple expedient of adding a potential flow $\boldsymbol{\nabla}\Psi$, with Ψ chosen so that both the conditions (1.5) and (1.6) are satisfied; this yields a two-parameter family of flows, namely

$$\boldsymbol{u}^{\mathrm{STF}} = (\alpha z - 8xy,\, 11x^2 + 3y^2 + z^2 + \beta xz - 3,\, -\alpha x + 2yz - \beta xy), \tag{1.7}$$

where the parameters α and β are related to the ratios of intensities of the stretch, twist and fold ingredients of the flow. It is easily seen that this flow is a particular example of the class (1.4), and that it satisfies the conditions (1.5) and (1.6). We have subjected this flow to detailed analytical and numerical investigation, and the results are illustrative of features that may be expected in the general case.

Although the present study is primarily kinematic in character, we may note at the outset that every flow of the form (1.4) is a solution of the Stokes equation

$$\nabla^2\boldsymbol{u}^{\mathrm{Q}} = \boldsymbol{\nabla}p \tag{1.8}$$

with $p = 2c_{ijj}x_i$. By the same token, the vorticity $\boldsymbol{\omega}^{\mathrm{Q}} = \boldsymbol{\nabla}\wedge\boldsymbol{u}^{\mathrm{Q}}$ is a linear function of $\boldsymbol{x}$ and satisfies

$$\nabla^2\boldsymbol{\omega}^{\mathrm{Q}} = 0. \tag{1.9}$$

This means that the flow (1.4) can, in principle, be realized as the unique Stokes flow of a viscous fluid in any domain D, provided $\boldsymbol{u}^{\mathrm{Q}}$ is prescribed in the form (1.4) on the boundary ∂D of the domain. We shall show, in §2 below, how the most general quadratic flow can (in principle) be realized when D is a sphere.

We should observe also that, although the terminology adopted in this paper is appropriate to the velocity in an incompressible fluid, the results are equally relevant to the problem of magnetic field structure $\boldsymbol{B}(\boldsymbol{x})$ in a plasma contained in a domain bounded by a perfect conductor on which $\boldsymbol{B}\cdot\boldsymbol{n}=0$. Any flow of the form (1.4) satisfying (1.5) and (1.6) can equally be interpreted as a magnetic field $\boldsymbol{B}^{\mathrm{Q}}(\boldsymbol{x})$ (not, in general, a magnetostatic equilibrium) in a spherical domain (a 'spheromak'). From this point of view, we may easily find topologically equivalent fields within ellipsoidal domains ('ellipsoidomaks'?). For consider the volume-preserving mapping $\boldsymbol{x}\rightarrow\boldsymbol{X}$, where

$$X_1 = s_1 x_1, \quad X_2 = s_2 x_2, \quad X_3 = s_3 x_3, \tag{1.10}$$

with $s_1 s_2 s_3 = 1$, which takes the sphere $x_1^2+x_2^2+x_3^2=1$ to the ellipsoid

$$\frac{X_1^2}{s_1^2}+\frac{X_2^2}{s_2^2}+\frac{X_3^2}{s_3^2}=1, \tag{1.11}$$

and which, under a frozen field distortion, converts a field $\boldsymbol{B}_0^{\mathrm{Q}}(\boldsymbol{x})$ to the form

$$B_i^{\mathrm{Q}}(\boldsymbol{X}) = B_{0j}^{\mathrm{Q}}(\boldsymbol{x})\frac{\partial X_i}{\partial x_j}, \tag{1.12}$$

i.e. $B_1^{\mathrm{Q}}(\boldsymbol{X}) = s_1 B_{01}^{\mathrm{Q}}(\boldsymbol{x})$, etc. If $\boldsymbol{B}_{0i}^{\mathrm{Q}}(\boldsymbol{x})$ is quadratic in $\boldsymbol{x}$ of the form (1.4), then $B_i^{\mathrm{Q}}(\boldsymbol{X})$ is quadratic in $\boldsymbol{X}$; in fact from (1.12)

$$B_i^{\mathrm{Q}}(\boldsymbol{X}) = s_{ij}(a_j+b_{jk}\sigma_{km}X_m+c_{jkl}\sigma_{km}\sigma_{ln}X_mX_n), \tag{1.13}$$

where

$$(s_{ij}) = \begin{pmatrix} s_1 & 0 & 0 \\ 0 & s_2 & 0 \\ 0 & 0 & s_3 \end{pmatrix}, \quad (\sigma_{ij}) = \begin{pmatrix} s_1^{-1} & 0 & 0 \\ 0 & s_2^{-1} & 0 \\ 0 & 0 & s_3^{-1} \end{pmatrix}. \tag{1.14}$$

Reinterpreting (1.13) as a velocity field, we have a means of determining a large family of Stokes flows within the ellipsoidal boundary (1.11). Of course, more general mappings $\boldsymbol{x}\rightarrow\boldsymbol{X}(\boldsymbol{x})$ will yield, via the Cauchy transformation (1.12), fields, and so flows, within domains that are arbitrary distortions of a sphere, but these will not be quadratic flows unless the mapping is linear.

In the following section, we obtain a complete classification of flows of the form (1.4) satisfying (1.5) and (1.6), and in §3 we describe the surface streamline topology of these flows on $r=1$. In §§4 and 5, we consider the question of integrability of the third-order dynamical system

$$\frac{\mathrm{d}\boldsymbol{x}}{\mathrm{d}t} = \boldsymbol{u}^{\mathrm{Q}}(\boldsymbol{x}), \tag{1.15}$$

and we show that the general quadratic flow can be expressed in different ways as the sum of two fields, each of which has closed streamlines within the sphere. This type of decomposition suggests an approach for analysis of the dynamical system (1.15), in terms of adiabatic invariants whose determination is essential to an understanding of the structure of Poincaré sections of the flow. The general technique is described in §6, and its application to the STF flow (1.7) is described in §7. The phenomenon of 'trans-adiabatic drift' whereby fluid particles can migrate from one adiabatic invariant surface to another, is identified and explained. Finally the results are summarized in §8.

2. Classification of quadratic flows in a sphere

Let us first rewrite (1.4) in the form

$$\boldsymbol{u}^{Q}(\boldsymbol{x}) = \boldsymbol{U}(\boldsymbol{x}) + \boldsymbol{V}(\boldsymbol{x}) + \boldsymbol{W}(\boldsymbol{x}), \tag{2.1}$$

where

$$U_i(\boldsymbol{x}) = a_i(1-2r^2) + (\boldsymbol{a}\cdot\boldsymbol{x})\,x_i, \tag{2.2}$$

$$V_i(\boldsymbol{x}) = b_{ij}\,x_j, \tag{2.3}$$

$$W_i(\boldsymbol{x}) = \tilde{c}_{ijk}\,x_j\,x_k, \tag{2.4}$$

and where

$$\tilde{c}_{ijk} = c_{ijk} + 2a_i\,\delta_{jk} + \tfrac{1}{2}(a_j\,\delta_{ik} + a_k\,\delta_{ij}) = \tilde{c}_{ikj}. \tag{2.5}$$

It may be easily verified that $\boldsymbol{U}(\boldsymbol{x})$ satisfies

$$\boldsymbol{\nabla}\cdot\boldsymbol{U} = 0 \quad \text{and} \quad \boldsymbol{U}\cdot\boldsymbol{x} = 0 \quad \text{on} \quad r = 1, \tag{2.6}$$

i.e. $\boldsymbol{U}(\boldsymbol{x})$ represents an incompressible flow in a sphere. Moreover, this flow is evidently axisymmetric about an axis through the centre of the sphere in the direction of the vector $\boldsymbol{a}$. If θ_a is the polar angle measured from this axis, then the Stokes stream function of this flow is given by

$$\psi(r,\theta_a) = \tfrac{1}{2}ar^2(1-r^2)\sin^2\theta_a, \tag{2.7}$$

whose streamlines are shown in figure 1. This is the (unique) Stokes flow that is 'driven' by a tangential velocity distribution $U_\theta = a\sin\theta_a$ on $r = 1$. It is the flow inside a buoyant spherical droplet (relative to its centre) rising at low Reynolds number in a viscous fluid (Batchelor 1967, p. 237). It is also the flow inside Hill's spherical vortex (Batchelor 1967, p. 526). We shall refer to $\boldsymbol{U}(\boldsymbol{x})$ as the *poloidal ingredient* of the flow $\boldsymbol{u}^{Q}(\boldsymbol{x})$.

Consider now the terms $\boldsymbol{V}$ and $\boldsymbol{W}$ of (2.1); since these are respectively linear and quadratic in x_i, they must separately satisfy conditions derived from (1.5) and (1.6), namely

$$\boldsymbol{\nabla}\cdot\boldsymbol{V} = 0, \quad \boldsymbol{V}\cdot\boldsymbol{x} = 0 \quad \text{on} \quad r = 1, \tag{2.8}$$

$$\boldsymbol{\nabla}\cdot\boldsymbol{W} = 0, \quad \boldsymbol{W}\cdot\boldsymbol{x} = 0 \quad \text{on} \quad r = 1. \tag{2.9}$$

It is easily shown that the only flow $\boldsymbol{V}$ of the form (2.3) satisfying (2.8) is the quasi-rigid rotation

$$\boldsymbol{V}(\boldsymbol{x}) = \boldsymbol{\Omega}\wedge\boldsymbol{x}, \tag{2.10}$$

with angular velocity $\Omega_i = -\tfrac{1}{2}\epsilon_{ijk}\,b_{jk}$.

Now $\boldsymbol{W}\cdot\boldsymbol{x} = \tilde{c}_{ijk}\,x_i\,x_j\,x_k = r^3F(\theta,\varphi)$ for some function $F(\theta,\varphi)$ of the spherical polar angles (θ,φ); and from (2.9), $F(\theta,\varphi) = 0$. Hence $\boldsymbol{W}\cdot\boldsymbol{x} = 0$ on every sphere $r = \text{const.}$, i.e. $\boldsymbol{W}(\boldsymbol{x})$ is a *toroidal* field expressible in the form

$$\boldsymbol{W} = \boldsymbol{\nabla}\wedge(\boldsymbol{x}T(\boldsymbol{x})) = -\boldsymbol{x}\wedge\boldsymbol{\nabla}T \tag{2.11}$$

for some scalar field $T(\boldsymbol{x})$ (see for example Moffatt 1978, §2.2). Since $\boldsymbol{W}$ is homogeneous quadratic in $\boldsymbol{x}$, T can be chosen quadratic and homogeneous also, i.e.

$$T = T_{ij}\,x_i\,x_j \tag{2.12}$$

for some symmetric matrix T_{ij}. Each term of this quadratic form yields a corresponding flow. For example, the flow corresponding to $T_{11}\,x^2$ is

$$\boldsymbol{W}_{11}(\boldsymbol{x}) = -\boldsymbol{x}\wedge\boldsymbol{\nabla}(T_{11}\,x^2) = 2T_{11}(0,-xz,xy). \tag{2.13}$$

This is a rotation about the x-axis with angular velocity $2T_{11}\,x$, linear in x; i.e. $\boldsymbol{W}_{11}(\boldsymbol{x})$

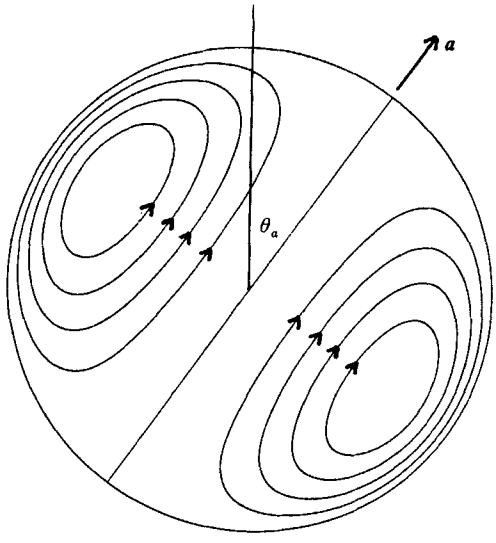

FIGURE 1. Streamlines $\psi(r, \theta_a) = \text{const.}$ of the flow (2.7) in the sphere $r < 1$.

is a *twist flow* with *rate of twist* $2T_{11}$ about the x-axis. Similarly for the terms $T_{22}y^2$ and $T_{33}z^2$.

The off-diagonal term $2T_{23}yz$ yields the flow

$$\boldsymbol{W}_{23}(\boldsymbol{x}) = -\boldsymbol{x} \wedge \boldsymbol{\nabla}(2T_{23}yz) = 2T_{23}(z^2-y^2, xy, -xz), \tag{2.14}$$

whose streamlines are the intersections of hyperbolic cylinder surfaces $yz = \text{const.}$ with spheres $r = \text{const.}$

Let us choose the principal axes of T_{ij} as axes $Oxyz$, and let $T^{(1)}, T^{(2)}, T^{(3)}$ be the eigenvalues of T_{ij}; then

$$T = T^{(1)}x^2 + T^{(2)}y^2 + T^{(3)}z^2, \tag{2.15}$$

and correspondingly

$$\boldsymbol{W}(\boldsymbol{x}) = (\lambda yz, \mu zx, \nu xy), \tag{2.16}$$

where $\lambda = 2(T^{(2)}-T^{(3)})$, $\mu = 2(T^{(3)}-T^{(1)})$, $\nu = 2(T^{(1)}-T^{(2)})$, so that

$$\lambda+\mu+\nu = 0. \tag{2.17}$$

Note that we may assume that $T^{(1)}$, $T^{(2)}$ and $T^{(3)}$ are all strictly positive, since we may add to T any multiple of $r^2 = x^2+y^2+z^2$ without changing $\boldsymbol{W}$ (since $\boldsymbol{x} \wedge \boldsymbol{\nabla}(r^2) = 0$). We may assume further, ignoring exceptional cases, that $T^{(1)} > T^{(2)} > T^{(3)}$, so that λ and ν are positive, and $\mu = -(\lambda+\nu)$ is negative. Then

$$\boldsymbol{W}(\boldsymbol{x}) = \lambda(yz, -zx, 0) + \nu(0, -zx, xy), \tag{2.18}$$

a superposition of two twists about the z-axis and the x-axis. We describe λ and ν as *the principal rates of twist*, and $\boldsymbol{W}(\boldsymbol{x})$ as the *twist ingredient* of the flow.

To summarize: we now have the general field $\boldsymbol{u}^{Q}(\boldsymbol{x})$ in the form

$$\boldsymbol{u}^{Q}(\boldsymbol{x}) = \boldsymbol{a}(1-2r^2) + (\boldsymbol{a}\cdot\boldsymbol{x})\,\boldsymbol{x} + \boldsymbol{\Omega} \wedge \boldsymbol{x} + (\lambda yz, \mu zx, \nu xy), \tag{2.19}$$

with $\lambda+\mu+\nu = 0$. There are eight independent parameters in the specification of the flow, namely

$$a_1, a_2, a_3, \Omega_1, \Omega_2, \Omega_3, \lambda, \nu. \tag{2.20}$$

Any one of these may be normalized to unity, leaving essentially seven parameters determining the flow structure.

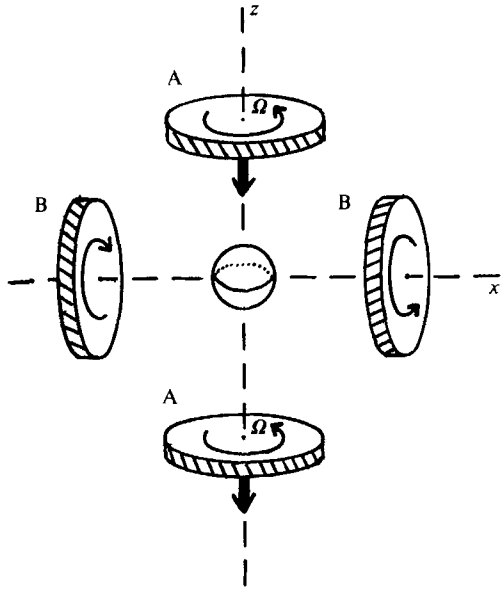

FIGURE 2. A thought-experiment whereby the Stokes flow (2.19) may be realized: a buoyant spherical droplet rises at low Reynolds number in a viscous fluid; the droplet is brought to rest by the downward motion of the corotating discs AA, which also generate the quasi-rigid rotation $\boldsymbol{\Omega}$; a twist ingredient is provided by discs BB counter-rotating about the x-axis; a second twist ingredient may be generated by similar discs counter-rotating about the y-axis.

The general toroidal flow $\boldsymbol{V}+\boldsymbol{W}$ may in principle be realized by a suitable distribution of rotating discs in the fluid. First, we place counter-rotating discs at opposite ends of two diameters to provide the twist flows parameterized by λ and ν; then we place corotating discs to provide the quasi-rigid rotation $\boldsymbol{\Omega}$. If a buoyant spherical droplet rises at low Reynolds number through this apparatus, then at the moment at which it passes through the centre, the velocity within it is given by (2.19). Alternatively, the corotating discs may be moved downwards to keep the droplet in fixed position, as indicated schematically for a particular case in figure 2.

3. Surface streamline topology

Since $\boldsymbol{u}^{\mathrm{Q}}\cdot\boldsymbol{x}=0$ on $r=1$, the flow is tangential on the unit sphere. Regarded as a surface flow, its surface divergence $\nabla_S\cdot\boldsymbol{u}^{\mathrm{Q}}$ is positive on the hemisphere where $\boldsymbol{a}\cdot\boldsymbol{x}>0$ (since there the poloidal ingredient of the flow approaches the surface from within and spreads out upon it) and negative on the hemisphere where $\boldsymbol{a}\cdot\boldsymbol{x}<0$.

Consider first just the twist flow $\boldsymbol{W}$, which has zero surface divergence. Its streamlines on $r=1$ are given by $T=\text{const.}$, i.e. they are the intersections of the family of ellipsoids,

$$T^{(1)}x^2+T^{(2)}y^2+T^{(3)}z^2=\text{const.}, \tag{3.1}$$

with the unit sphere. Figure 3(a) shows the situation when, as assumed above, $T^{(1)}>T^{(2)}>T^{(3)}$, so that $\lambda,\nu>0,\mu<0$. There are four elliptic (or 'O-type') stagnation points where the x- and z-axes intersect the sphere, and two hyperbolic (or 'X-type') stagnation points where the y-axis intersects the sphere. Note that if we assign an index (or rotation number) $+1$ to each O-type stagnation point, and -1 to each X-type stagnation point, then the sum of the six indices is $+2$, the Euler

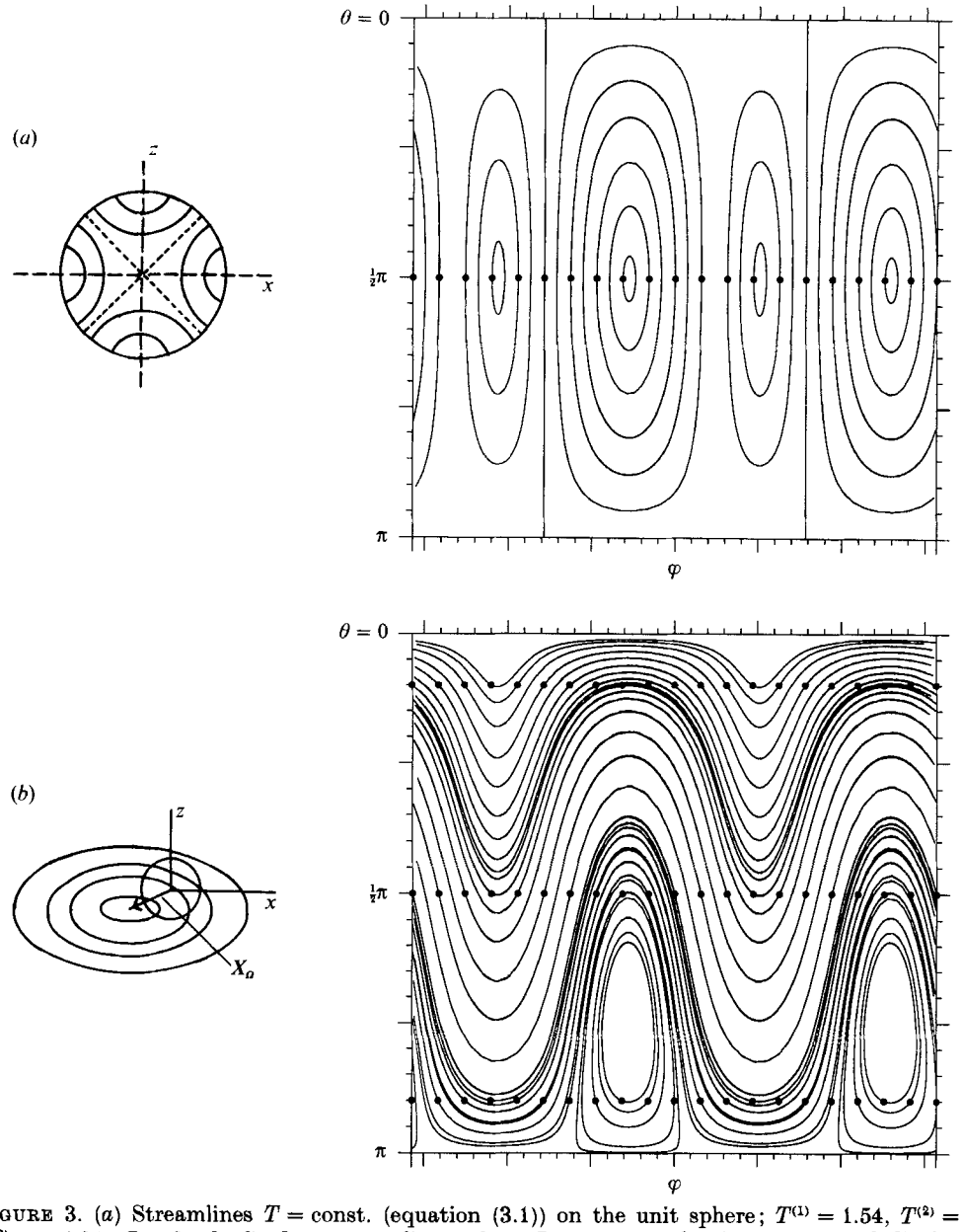

FIGURE 3. (*a*) Streamlines $T = \text{const.}$ (equation (3.1)) on the unit sphere; $T^{(1)} = 1.54$, $T^{(2)} = 0$, $T^{(3)} = -4.04$, $\boldsymbol{\Omega} = 0$. (*b*) Surface streamlines when $\boldsymbol{\Omega} \neq 0$, given by intersection of displaced ellipsoids (3.2) with the sphere $r = 1$; $\boldsymbol{\Omega} = (0, 4, 0)$. On the left is the construction described in the text; on the right are the streamlines in Mercator's projection. ($x = \sin\theta \sin\phi, y = \cos\theta$, $z = \sin\theta\cos\phi$.)

characteristic (and a topological invariant) for the sphere (see, for example, Arnol'd 1973, p. 260).

The quasi-rigid rotation $\boldsymbol{V}(\boldsymbol{x}) = \boldsymbol{\Omega} \wedge \boldsymbol{x} = \boldsymbol{\nabla} \wedge [\boldsymbol{x}(\boldsymbol{\Omega}\cdot\boldsymbol{x})]$ is of course also toroidal, and the composite flow $\boldsymbol{V} + \boldsymbol{W}$ has surface streamlines given by the intersections of the 'displaced' ellipsoids:

$$T_c = T^{(1)}x^2 + T^{(2)}y^2 + T^{(3)}z^2 + \boldsymbol{\Omega}\cdot\boldsymbol{x} = \text{const.} \tag{3.2}$$

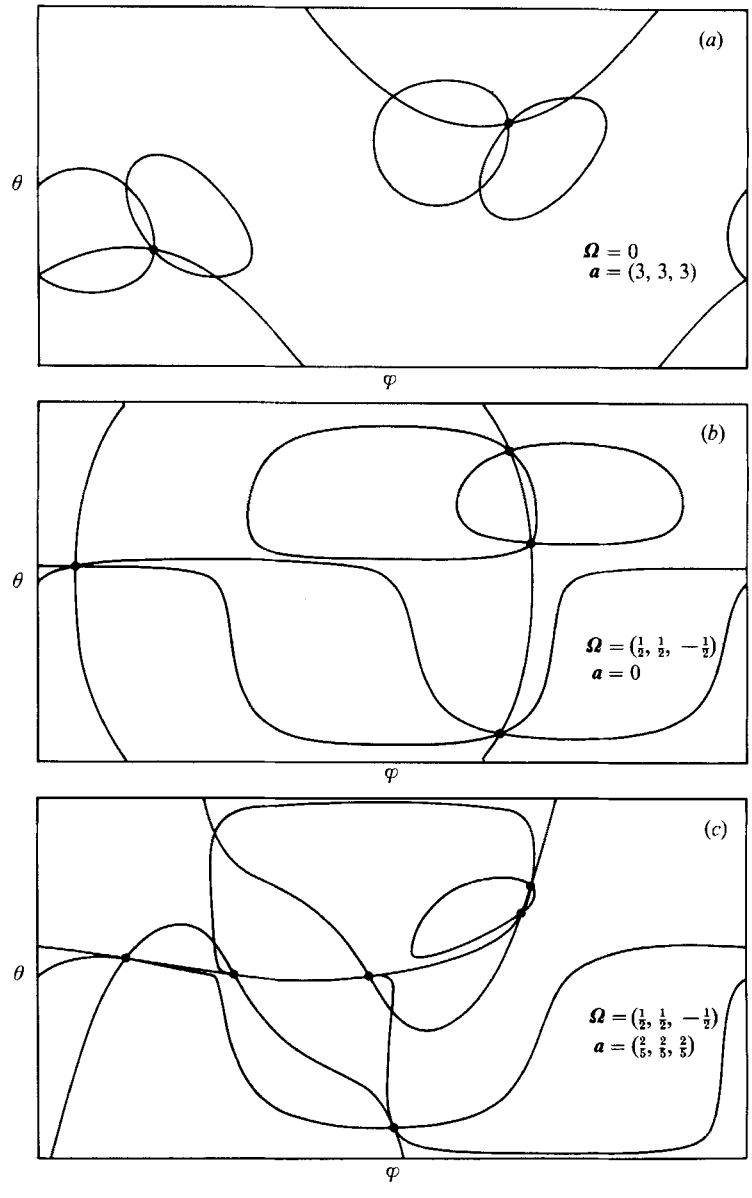

FIGURE 4. Curves on which the Cartesian components u, v and w, vanish on $r = 1$; stagnation points correspond to the triple intersections identified by ●.

with the sphere $r = 1$, the centre of these displaced ellipsoids being at the point

$$\boldsymbol{X}_{\boldsymbol{\Omega}} = -\frac{1}{2}\left(\frac{\Omega_1}{T^{(1)}}, \frac{\Omega_2}{T^{(2)}}, \frac{\Omega_3}{T^{(3)}}\right). \tag{3.3}$$

From a purely geometric point of view, this is equivalent to displacement of the sphere $r = 1$ relative to the ellipsoids through $-\boldsymbol{X}_{\boldsymbol{\Omega}}$. Again the situation is easily visualized as in figure 3(*b*). Evidently if we increase $|\boldsymbol{\Omega}|$ keeping the direction of $\boldsymbol{\Omega}$ fixed, the X-type and O-type stagnation points disappear in pairs when in effect the rotation flow $\boldsymbol{V}$ dominates over the twist flow $\boldsymbol{W}$, finally leaving just two O-type

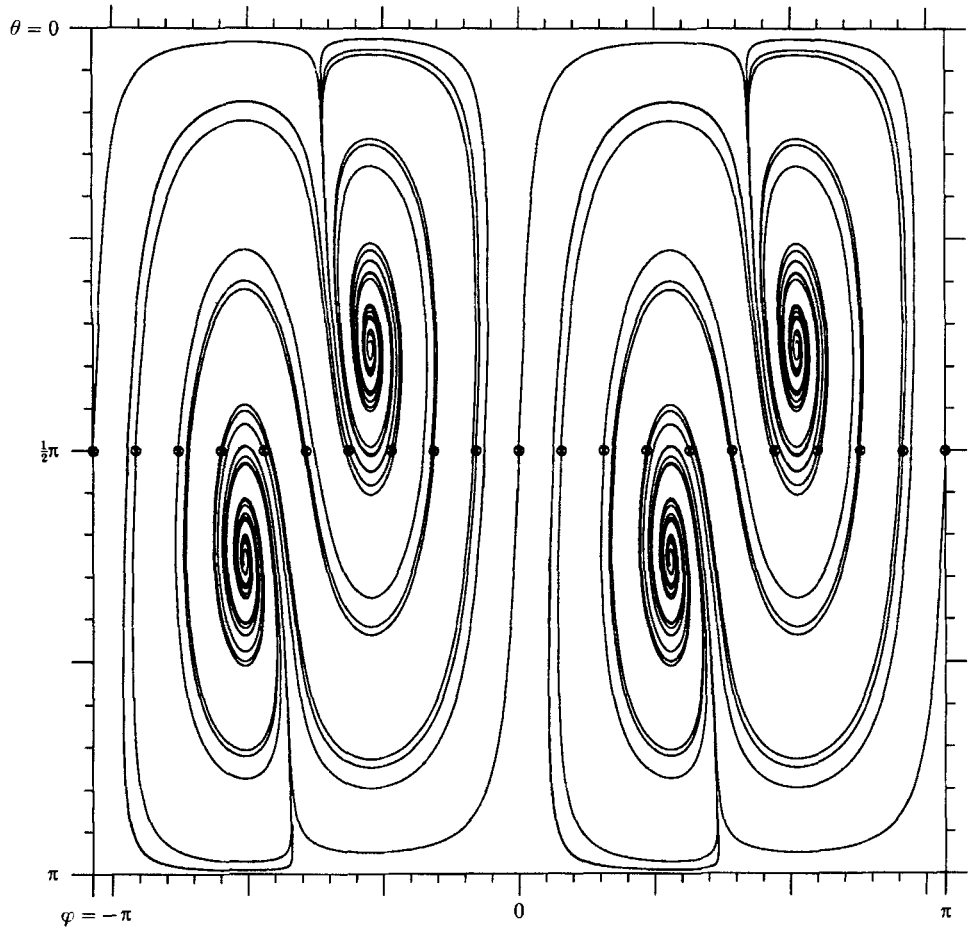

FIGURE 5. Surface streamline pattern for STF flow (1.7) with $\alpha = -1$, $\beta = 0.25$. There are four spirals, and two saddles (at $\theta = 0, \pi$).

stagnation points, as for a quasi-rigid rotation alone. At each stage, the sum of the indices of the stagnation points remains equal to $+2$, as it must.

Superposition of the poloidal ingredient $\boldsymbol{U}(\boldsymbol{x})$ now complicates the situation further, particularly through the introduction of the surface divergence referred to above. This converts O-type neutral points to 'spirals', converging or diverging according as they are on the hemispheres where $\boldsymbol{a}\cdot\boldsymbol{x} < 0$ or > 0 respectively.

The stagnation points may be located by evaluating the Cartesian components $u(\theta,\varphi), v(\theta,\varphi), w(\theta,\varphi)$ as functions of θ and φ on $r = 1$, and plotting the curves $u = 0, v = 0, w = 0$. The stagnation points are the points where all three curves intersect. (Note that, except at points on the three equators $\theta = \frac{1}{2}\pi$, $\varphi = 0, \pi$, and $\varphi = \frac{1}{2}\pi, \frac{3}{2}\pi$, an intersection of two of the curves implies a triple intersection since $\boldsymbol{u}\cdot\boldsymbol{n} = 0$.) Figure 4 shows three fairly typical situations, in which two, four and six stagnation points are located. We have not found any values of the parameters that give eight stagnation points, although this is not excluded on topological grounds.

Figure 5 shows the actual surface streamlines for the STF flow (1.7), with $\alpha = -1$, $\beta = 0.25$. Four spirals are evident, and there are two saddles at the poles, $\theta = 0$, $\theta = \pi$.

4. Streamline helicity

Let $\boldsymbol{A}^{\mathrm{Q}}(\boldsymbol{x})$ be a vector potential for $\boldsymbol{u}^{\mathrm{Q}}(\boldsymbol{x})$; then we may define the *streamline helicity* of the flow $\boldsymbol{u}^{\mathrm{Q}}$ by

$$H_{\mathrm{S}} = \int_{r<1} \boldsymbol{u}^{\mathrm{Q}} \cdot \boldsymbol{A}^{\mathrm{Q}} \, \mathrm{d}V, \tag{4.1}$$

a quantity that is independent of the gauge of $\boldsymbol{A}^{\mathrm{Q}}$ by virtue of (1.6). H_{S} provides a measure of the net streamline linkage within the sphere (Moffatt 1969) and is therefore of some relevance for what follows. Note that H_{S} is different from the usual helicity H of a flow defined by

$$H = \int_D \boldsymbol{u} \cdot \boldsymbol{\omega} \, \mathrm{d}V, \tag{4.2}$$

where $\boldsymbol{\omega} = \boldsymbol{\nabla} \wedge \boldsymbol{u}$; H provides a measure of the degree of linkage of *vortex* lines within D provided $\boldsymbol{\omega} \cdot \boldsymbol{n} = 0$ on ∂D. H is not relevant in the present context, but H_{S} is. (Note that H_{S} is invariant under frozen field distortions of the type (1.12) with $\boldsymbol{B}^{\mathrm{Q}}$ replaced by $\boldsymbol{u}^{\mathrm{Q}}$.)

In order to calculate H_{S}, note first that the decomposition of $\boldsymbol{A}^{\mathrm{Q}}$ corresponding to the decomposition (2.1) is

$$\boldsymbol{A}^{\mathrm{Q}} = \boldsymbol{A}_1(\boldsymbol{x}) + \boldsymbol{A}_2(\boldsymbol{x}) + \boldsymbol{A}_3(\boldsymbol{x}), \tag{4.3}$$

where

$$\boldsymbol{A}_1(\boldsymbol{x}) = \tfrac{1}{2}(\boldsymbol{a} \wedge \boldsymbol{x})(1 - r^2), \tag{4.4}$$

$$\boldsymbol{A}_2(\boldsymbol{x}) = \tfrac{1}{5}[(\boldsymbol{\Omega} \cdot \boldsymbol{x})\boldsymbol{x} - \boldsymbol{\Omega} r^2], \tag{4.5}$$

$$\boldsymbol{A}_3(\boldsymbol{x}) = \boldsymbol{x}(T^{(1)}x^2 + T^{(2)}y^2 + T^{(3)}z^2). \tag{4.6}$$

Now $\int \boldsymbol{U} \cdot \boldsymbol{A}_1 \, \mathrm{d}V = 0$, since $\boldsymbol{U} \cdot \boldsymbol{A}_1$ vanishes identically, and the integration is throughout a sphere; this is of course consistent with the fact that the streamlines of $\boldsymbol{U}$ are closed curves which are unlinked. Similarly, the streamlines of $\boldsymbol{V} + \boldsymbol{W}$ are closed curves on spheres $r = \text{const.}$ and are therefore also unlinked; hence $\int (\boldsymbol{V} + \boldsymbol{W}) \cdot (\boldsymbol{A}_2 + \boldsymbol{A}_3) \mathrm{d}V = 0$, as may be verified by explicit calculation. Moreover $\boldsymbol{U} \cdot \boldsymbol{A}_3$ is an odd function of (x, y, z) so that

$$\int \boldsymbol{U} \cdot \boldsymbol{A}_3 \, \mathrm{d}V = \int \boldsymbol{W} \cdot \boldsymbol{A}_1 \, \mathrm{d}V = 0 \tag{4.7}$$

also; in this case, the streamlines of $\boldsymbol{U}$ and $\boldsymbol{W}$ *are* linked, but positive linkages cancel negative linkages. This then leaves

$$H_S = \int (\boldsymbol{U} \cdot \boldsymbol{A}_2 + \boldsymbol{V} \cdot \boldsymbol{A}_1) \, \mathrm{d}V = 2 \int \boldsymbol{U} \cdot \boldsymbol{A}_2 \, \mathrm{d}V. \tag{4.8}$$

Substituting from (2.2) and (4.5), and evaluating the integral, we find

$$H_S = \frac{16\pi}{105} \boldsymbol{\Omega} \cdot \boldsymbol{a}. \tag{4.9}$$

Non-zero streamline helicity corresponds to the evident linkage of the streamlines of $\boldsymbol{U}$ and $\boldsymbol{V}$ when $\boldsymbol{\Omega} \cdot \boldsymbol{a} \neq 0$.

This situation is most easily visualized when $\boldsymbol{\Omega}$ is parallel to $\boldsymbol{a}$ so that the streamlines of $\boldsymbol{U} + \boldsymbol{V}$ then lie on the family of nested tori

$$\psi(r, \theta_a) = \psi_0 (= \text{const.}) \quad (0 < \psi_0 < \tfrac{1}{8}a), \tag{4.10}$$

where $\psi(r, \theta_a)$ is the Stokes stream function (2.7). The streamlines are generally

ergodic on these surfaces but may be closed in the form of torus knots for particular values of ψ_0.

5. Alternative decomposition of u^Q as the sum of two flows with closed streamlines

We have seen in §2 that the general quadratic flow $\boldsymbol{u}^Q$ can be decomposed into the sum of poloidal and toroidal parts $\boldsymbol{u}_P = \boldsymbol{U}$, $\boldsymbol{u}_T = \boldsymbol{V} + \boldsymbol{W}$, each of which separately has closed streamlines. There is another type of decomposition which has the same property, and which is useful in analysing the STF flow. This is now described.

Let us write the general flow (2.19) in the form

$$\boldsymbol{u}^Q = \boldsymbol{u}_1(\boldsymbol{x}) + \boldsymbol{u}_2(\boldsymbol{x}), \tag{5.1}$$

where
$$\boldsymbol{u}_1 = \boldsymbol{a}_1(1-2r^2) + (\boldsymbol{a}_1 \cdot \boldsymbol{x})\boldsymbol{x} + \boldsymbol{\Omega}_1 \wedge \boldsymbol{x} + (\lambda yz, \mu zx, \nu xy), \tag{5.2}$$

$$\boldsymbol{u}_2 = \boldsymbol{a}_2(1-2r^2) + (\boldsymbol{a}_2 \cdot \boldsymbol{x})\boldsymbol{x} + \boldsymbol{\Omega}_2 \wedge \boldsymbol{x}, \tag{5.3}$$

with
$$\left.\begin{aligned} \boldsymbol{a}_1 &= (0, a_2, 0), \quad \boldsymbol{a}_2 = (a_1, 0, a_3), \\ \boldsymbol{\Omega}_1 &= (\Omega_1, 0, \Omega_3), \quad \boldsymbol{\Omega}_2 = (0, \Omega_2, 0). \end{aligned}\right\} \tag{5.4}$$

Note that $\boldsymbol{a}_1 \cdot \boldsymbol{\Omega}_1 = \boldsymbol{a}_2 \cdot \boldsymbol{\Omega}_2 = 0$, so that the streamline helicities of $\boldsymbol{u}_1$ and $\boldsymbol{u}_2$ are separately zero. Note further that we have chosen $\boldsymbol{a}_1$ and $\boldsymbol{\Omega}_2$ to be the projections of $\boldsymbol{a}$ and $\boldsymbol{\Omega}$ along the principal direction of twist corresponding to the negative twist parameter $\mu = -(\lambda + \nu)$; this is the essence of the decomposition (5.1).

Consider first the structure of the flow $\boldsymbol{u}_1$. Its streamlines are given by

$$\frac{\mathrm{d}x}{a_2 x - \Omega_3 + \lambda z} = \frac{y\,\mathrm{d}y}{a_2(1-2r^2) + a_2 y^2 + \Omega_3 x - \Omega_1 z + \mu zx} = \frac{\mathrm{d}z}{a_2 z + \Omega_1 + \nu x}, \tag{5.5}$$

a system that is symmetric about the plane $y = 0$, and integrable as follows. Let (x_0, z_0) be the solution of †

$$a_2 x_0 - \Omega_3 + \lambda z_0 = 0, \quad a_2 z_0 + \Omega_1 + \nu x_0 = 0, \tag{5.6}$$

i.e.
$$x_0 = \frac{a_2\Omega_3 - \lambda\Omega_1}{a_2^2 - \lambda\nu}, \quad z_0 = \frac{-a_2\Omega_1 - \nu\Omega_3}{a_2^2 - \lambda\nu}, \tag{5.7}$$

and let $x = x_0 + X$, $z = z_0 + Z$. Then from the first and third terms of (5.5) we have

$$\frac{\mathrm{d}X}{a_2 X + \lambda Z} = \frac{\mathrm{d}Z}{a_2 Z + \nu X} = \frac{\mathrm{d}(pX + qZ)}{(a_2 p + \nu q)X + (\lambda p + a_2 q)Z}. \tag{5.8}$$

We choose p and q so that

$$a_2 p + \nu q = \sigma p, \quad \lambda p + a_2 q = \sigma q, \tag{5.9}$$

i.e.
$$\sigma = \sigma_1 = a_2 + (\lambda\nu)^{\frac{1}{2}}, \quad p/q = (\nu/\lambda)^{\frac{1}{2}}, \tag{5.10}$$

or
$$\sigma = \sigma_2 = a_2 - (\lambda\nu)^{\frac{1}{2}}, \quad p/q = -(\nu/\lambda)^{\frac{1}{2}}. \tag{5.11}$$

The integral curves of (5.8) follow in the form

$$(\nu^{\frac{1}{2}}X - \lambda^{\frac{1}{2}}Z)^{\sigma_1}(\nu^{\frac{1}{2}}X + \lambda^{\frac{1}{2}}Z)^{-\sigma_2} = \text{const.} \tag{5.12}$$

† The case $a_2^2 = \lambda\nu$ requires special treatment; the details are omitted.

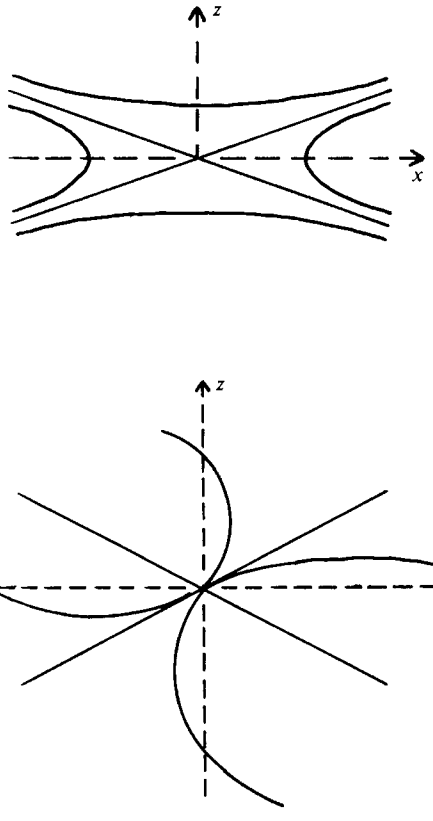

FIGURE 6. The curves (5.12). (*a*) Quasi-hyperbolic ($\lambda\nu > a_2^2$); (*b*) quasi-parabolic ($\lambda\nu < a_2^2$).

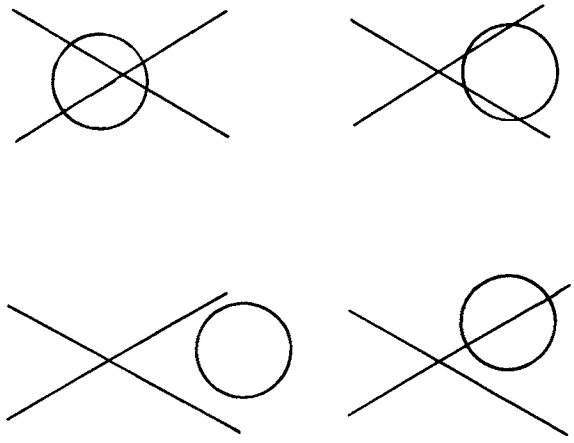

FIGURE 7. Four distinct possibilities for the position of the invariant planes $\nu^{\frac{1}{2}}X = \pm\lambda^{\frac{1}{2}}Z$ relative to the sphere $r = 1$.

The form of these curves is sketched in figure 6; they may be described as 'quasi-hyperbolic' or 'quasi-parabolic' according as $\sigma_1\sigma_2 < 0$ or > 0, i.e. according as

$$\lambda\nu > a_2^2 \quad \text{or} \quad \lambda\nu < a_2^2. \tag{5.13}$$

The streamlines of $\boldsymbol{u}_1$ must then be closed curves lying on the parts of the

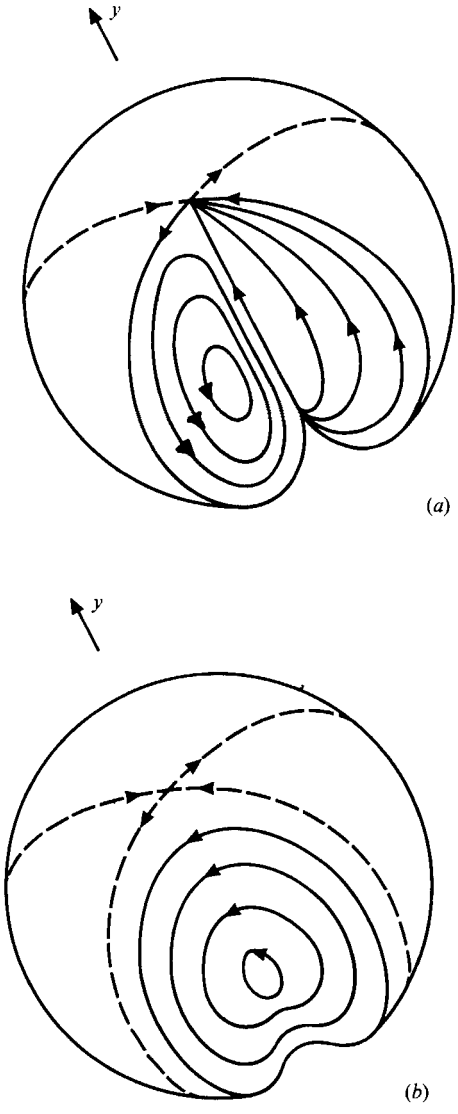

FIGURE 8. (*a*) Perspective view of the streamlines on the invariant planes, and (*b*) streamlines on one of the surfaces (5.12), when $\Omega_1 = \Omega_3 = 0$ and $\lambda\nu > a_2^2$.

cylindrical surfaces (5.12) (now reinterpreted in three dimensions) lying inside the sphere $r = 1$. In particular, the planes $\nu^{\frac{1}{2}}X = \pm\lambda^{\frac{1}{2}}Z$ are invariant planes of the flow. There are a number of distinct topologies according to the position of these planes relative to the sphere $r = 1$ (figure 7).

The case when $\Omega_1 = \Omega_3 = 0$ is of particular interest for the sequel. The invariant planes then intersect at $x = z = 0$. In this case, let

$$\xi = \nu^{\frac{1}{2}}x - \lambda^{\frac{1}{2}}z, \quad \zeta = \nu^{\frac{1}{2}}x + \lambda^{\frac{1}{2}}z. \tag{5.14}$$

Then the integral curves in the invariant plane $\zeta = 0$ are, from (5.5), given by

$$\frac{y\,\mathrm{d}y}{a_2(1-y^2)-\delta\xi^2} = \frac{\mathrm{d}\xi}{\sigma_2\xi}, \tag{5.15}$$

where
$$\delta = \tfrac{1}{2}a_2\left(\frac{1}{\lambda}+\frac{1}{\nu}\right)+\frac{\mu}{4(\lambda\nu)^{\frac{1}{2}}}. \tag{5.16}$$

This may be solved explicitly. There are singular points at $\xi = 0$, $y = \pm 1$. Putting $y = \pm 1 + \eta$ and linearizing, we find that the integral curves near these points are of the form
$$\eta^{\sigma_2}\xi^{2a_2} = \text{const.} \tag{5.17}$$

Similarly the integral curves in the invariant plane $\xi = 0$ have singular points at $\zeta = 0$, $y = \pm 1$, and near these points have the form
$$\eta^{\sigma_1}\zeta^{2a_2} = \text{const.} \tag{5.18}$$

Both families (5.17) and (5.18) are quasi-hyperbolic if $\sigma_1\sigma_2 = a_2^2 - \lambda\nu > 0$, but if $a_2^2 < \lambda\nu$ then one family is quasi-hyperbolic and one is quasi-parabolic (which is which depending on the sign of a_2). The form of the streamlines in this latter situation is sketched in figure 8.

The main point however is that in all cases the streamlines of $\boldsymbol{u}_1$ are unlinked closed curves†, consistent with (although not implied by) the zero streamline helicity of $\boldsymbol{u}_1$. Similarly, and *a fortiori*, the streamlines of the field $\boldsymbol{u}_2(\boldsymbol{x})$ (equation (5.3)) are unlinked closed curves as may be seen by choosing new axes $Ox'yz'$ with Ox' aligned along $\boldsymbol{a}_2$.

We have thus achieved a decomposition of the general quadratic flow (2.19) into the sum of two flows $\boldsymbol{u}_1(\boldsymbol{x})$ and $\boldsymbol{u}_2(\boldsymbol{x})$ each of which separately has closed unlinked streamlines. There is of course in general a cross-linkage of the streamlines of $\boldsymbol{u}_1$ and $\boldsymbol{u}_2$ which is associated with the streamline helicity of the total field $\boldsymbol{u}^{\mathrm{Q}}$.

6. Adiabatic invariants for weakly perturbed closed-streamline flow

The foregoing discussion suggests that it may be useful to consider flows of the form
$$\boldsymbol{u}^{\mathrm{Q}}(\boldsymbol{x}) = \boldsymbol{u}_1(\boldsymbol{x}) + \epsilon\boldsymbol{u}_2(\boldsymbol{x}), \tag{6.1}$$
where $\boldsymbol{u}_1(\boldsymbol{x})$ is an unperturbed quadratic flow having closed streamlines, $\boldsymbol{u}_2(\boldsymbol{x})$ is an arbitrary quadratic flow, and $\epsilon \ll 1$. For example, $\boldsymbol{u}_1(\boldsymbol{x})$ may be the flow (5.2) whose streamlines are the intersections within the sphere $r = 1$ of two families of cylindrical surfaces obtained by integration of (5.5), say
$$I(x,z) = \text{const.}, \quad J(y,z) = \text{const.} \tag{6.2}$$

The invariant $I(x,z)$ can be obtained explicitly, as in (5.12), and the invariant $J(y,z)$ can be obtained in principle by then eliminating x from (5.5) to give an equation of the form $\mathrm{d}y/\mathrm{d}z = G(y,z)$, and by numerical integration.

The closed streamlines are then 'labelled' by particular values of the invariants I and J, and position on the streamline may be labelled by an angular coordinate φ ($0 \leqslant \varphi < 2\pi$). Adopting I, J, φ as new variables, the dynamical system associated with the flow (6.1), namely
$$\frac{\mathrm{d}\boldsymbol{x}}{\mathrm{d}t} = \boldsymbol{u}_1(\boldsymbol{x}) + \epsilon\boldsymbol{u}_2(\boldsymbol{x}), \tag{6.3}$$

† Except possibly in one of the invariant planes where, if $\sigma_1\sigma_2 < 0$, the streamlines are heteroclinic lines joining the singular points at $y = \pm 1$.

must convert to the form

$$\left.\begin{aligned}\frac{\mathrm{d}I}{\mathrm{d}t} &= \epsilon F(I,J,\varphi),\\ \frac{\mathrm{d}J}{\mathrm{d}t} &= \epsilon G(I,J,\varphi),\\ \frac{\mathrm{d}\varphi}{\mathrm{d}t} &= \omega(I,J)+\epsilon H(I,J,\varphi),\end{aligned}\right\} \tag{6.4}$$

since I and J are invariant when $\epsilon = 0$. The first-order variation of I and J is then obtained by replacing F and G by their orbital averages over φ

$$\bar{F}(I,J) = \frac{1}{2\pi}\int_0^{2\pi} F(I,J,\varphi)\,\mathrm{d}\varphi, \quad \bar{G}(I,J) = \frac{1}{2\pi}\int_0^{2\pi} G(I,J,\varphi)\,\mathrm{d}\varphi \tag{6.5}$$

(for a discussion of this 'principle of averaging' see Arnol'd 1978 §52). Then, with $\tau = \epsilon t$,

$$\frac{\mathrm{d}I}{\mathrm{d}\tau} = \bar{F}(I,J), \quad \frac{\mathrm{d}J}{\mathrm{d}\tau} = \bar{G}(I,J). \tag{6.6}$$

The integral curves of this second-order system are of the form

$$A(I,J) = \text{const.} \tag{6.7}$$

and the function $A(I,J)$ is an 'adiabatic invariant' of the flow. Using (6.2), this may be expressed as a function of (x,y,z):

$$A(I,J) = \mathscr{A}(x,y,z), \tag{6.8}$$

say, and the system may be expected to evolve on the surfaces $\mathscr{A} = \text{const.}$ for times τ of order unity, i.e. for $t = O(\epsilon^{-1})$.

We shall now apply this technique to the STF flow (1.7), treating α as the parameter which may be small or large, and we compare the predictions with the results of numerical integration.

7. The stretch–twist–fold (STF) flow

Following the notation of §§5 and 6, we may express the flow (1.7) in the form

$$\boldsymbol{u} = \boldsymbol{u}_1(\boldsymbol{x}) + \alpha \boldsymbol{u}_2(\boldsymbol{x}), \tag{7.1}$$

where

$$\boldsymbol{u}_2(\boldsymbol{x}) = (z, 0, -x), \tag{7.2}$$

a quasi-rigid rotation about the axis Oy, and

$$\boldsymbol{u}_1(\boldsymbol{x}) = (-8xy,\ 11x^2+3y^2+z^2+\beta xz-3,\ 2yz-\beta xy). \tag{7.3}$$

This is a flow of type $\boldsymbol{U}+\boldsymbol{W}$, in the notation of §2, with

$$\boldsymbol{a} = (0,-3,0), \quad (T_{ij}) = \begin{pmatrix} -\frac{1}{2}\beta & 0 & \frac{5}{2} \\ 0 & 0 & 0 \\ \frac{5}{2} & 0 & 0 \end{pmatrix}. \tag{7.4}$$

The vector $\boldsymbol{a}$ is in the direction Oy, which is clearly one of the principal directions of the twist matrix T_{ij}. Hence the decomposition (7.1) is of the type (5.1)–(5.4), and the

structure of $\boldsymbol{u}_1(\boldsymbol{x})$ is precisely as described for the more general flow (5.2) with $\boldsymbol{\Omega} = 0$. The eigenvalues of T_{ij} are

$$T^{(1)} = \tfrac{1}{2}[(\tfrac{1}{2}\beta)^2+25]^{\frac{1}{2}}-\tfrac{1}{4}\beta, \quad T^{(2)} = 0, \quad T^{(3)} = -\tfrac{1}{2}[(\tfrac{1}{2}\beta)^2+25)^{\frac{1}{2}}-\tfrac{1}{4}\beta$$

and correspondingly

$$\lambda = \tfrac{1}{2}[(\beta^2+100)^{\frac{1}{2}}+\beta], \quad \mu = -(\beta^2+100)^{\frac{1}{2}}, \quad \nu = \tfrac{1}{2}[(\beta^2+100)^{\frac{1}{2}}-\beta]$$

so that $\lambda\nu = 25$, and so from (5.10), (5.11),

$$\sigma_1 = 2, \quad \sigma_2 = -8,$$

independent of the value of β. Since $\sigma_1\sigma_2 < 0$, the streamlines on the invariant planes have the structure described by figure 8(*a*). The integral (5.12) takes the form

$$I = x(z-\tfrac{1}{10}\beta x)^4 = \text{const.}, \tag{7.5}$$

as may be easily verified directly from the dynamical system associated with (7.3).

7.1. *The case* $\alpha \gg 1$

In this limit, we write (7.1) in the form

$$\epsilon\boldsymbol{u} = \boldsymbol{u}_2(\boldsymbol{x})+\epsilon\boldsymbol{u}_1(\boldsymbol{x}) \tag{7.6}$$

with $\epsilon = \alpha^{-1}$, and apply the technique of §6. The streamlines of $\boldsymbol{u}_2$ are the circles

$$y = \text{const.}, \quad x^2+z^2 = \text{const.}, \tag{7.7}$$

and these provide the 'zero-order' invariants $I(= x^2+z^2)$ and $J(= y)$. The angle φ is just the azimuth angle around the axis Oy, and the system (6.6) takes the form

$$\frac{\mathrm{d}J}{\mathrm{d}\tau} = 3J^2+6I-3, \quad \frac{\mathrm{d}I}{\mathrm{d}\tau} = -6IJ, \tag{7.8}$$

with integral curves

$$A(I,J) = I(J^2+I-1) \quad \text{or} \quad \mathscr{A}(x,y,z) = (x^2+z^2)(x^2+y^2+z^2-1). \tag{7.9}$$

As explained in §6 this is an adiabatic invariant for the flow (7.6). We notice that $\mathscr{A}$ is equal to the stream function of the Hill's vortex (2.7) (see figure 1). It is now evident that averaging the perturbation field $\epsilon\boldsymbol{u}_1(\boldsymbol{x})$ over the orbits of the main ingredient $\boldsymbol{u}_2$ of the flow (7.6) simply eliminates the twist ingredients and leaves the axisymmetric (poloidal) ingredient. We should stress that in order to average the perturbation we first had to write the dynamical system associated with (7.6) in 'slow variables' I, J. One can easily check that averaging the *Cartesian* components of $\epsilon\boldsymbol{u}_1(\boldsymbol{x})$ over the polar angle ϕ gives the wrong answer.

The dynamical system

$$\frac{\mathrm{d}\boldsymbol{x}}{\mathrm{d}t} = \boldsymbol{u}_2(\boldsymbol{x})+\epsilon\boldsymbol{u}_1(\boldsymbol{x}) \tag{7.10}$$

has been integrated with $\beta = 1$ and $\epsilon = 1/700 = 0.00143$, for a number (20) of initial conditions, and the Poincaré sections on the plane $x = z$ are shown in figure 9. Each trajectory is represented by 5000 points of section. These lie on curves which are indistinguishable from the streamlines of the flow (2.7), thus confirming that the associated adiabatic invariant (7.9) does indeed provide an excellent description of the behaviour when ϵ is small.

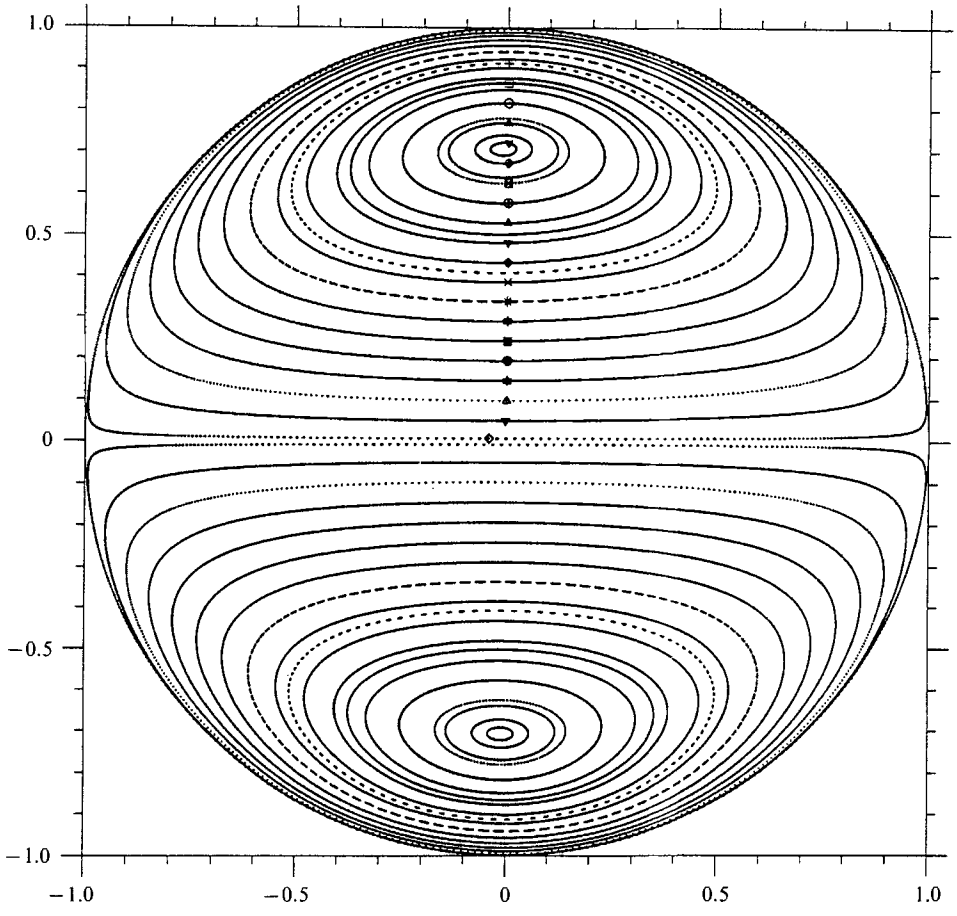

FIGURE 9. Poincaré sections (plane $x = z$) associated with 20 trajectories of the flow (1.7) with $\alpha = \epsilon^{-1} = 700$ and $\beta = 1$. 5000 points of section are plotted for each streamline; these lie on closed curves which are indistinguishable from the curves $\mathscr{A}(x, y, x) = 2x^2(2x^2 + y^2 - 1) = \text{const.}$ (equation (7.9) and figure 1). The curves that have a dotted or dashed appearance correspond to near-rational winding numbers on the corresponding tori.

7.2. *The case* $\alpha \ll 1$

Here the behaviour is more subtle. The unperturbed flow has the primary invariant (7.5) but the second invariant cannot in general be found explicitly. When $\beta = 0$, however, some analytical progress can be made, and this case turns out in fact to be quite typical. In this case, the unperturbed dynamical system ($\alpha = \beta = 0$) is

$$\frac{\mathrm{d}x}{\mathrm{d}t} = -8xy, \quad \frac{\mathrm{d}y}{\mathrm{d}t} = 11x^2 + 3y^2 + z^2 - 3, \quad \frac{\mathrm{d}z}{\mathrm{d}t} = 2yz, \tag{7.11}$$

and the invariant (7.5) is

$$I = xz^4, \tag{7.12}$$

so that the invariant planes are $x = 0$, $z = 0$. Moreover, since

$$r\frac{\mathrm{d}r}{\mathrm{d}t} = \boldsymbol{x}\cdot\frac{\mathrm{d}\boldsymbol{x}}{\mathrm{d}t} = 3y(r^2 - 1) = \frac{3}{2z}\frac{\mathrm{d}z}{\mathrm{d}t}(r^2 - 1), \tag{7.13}$$

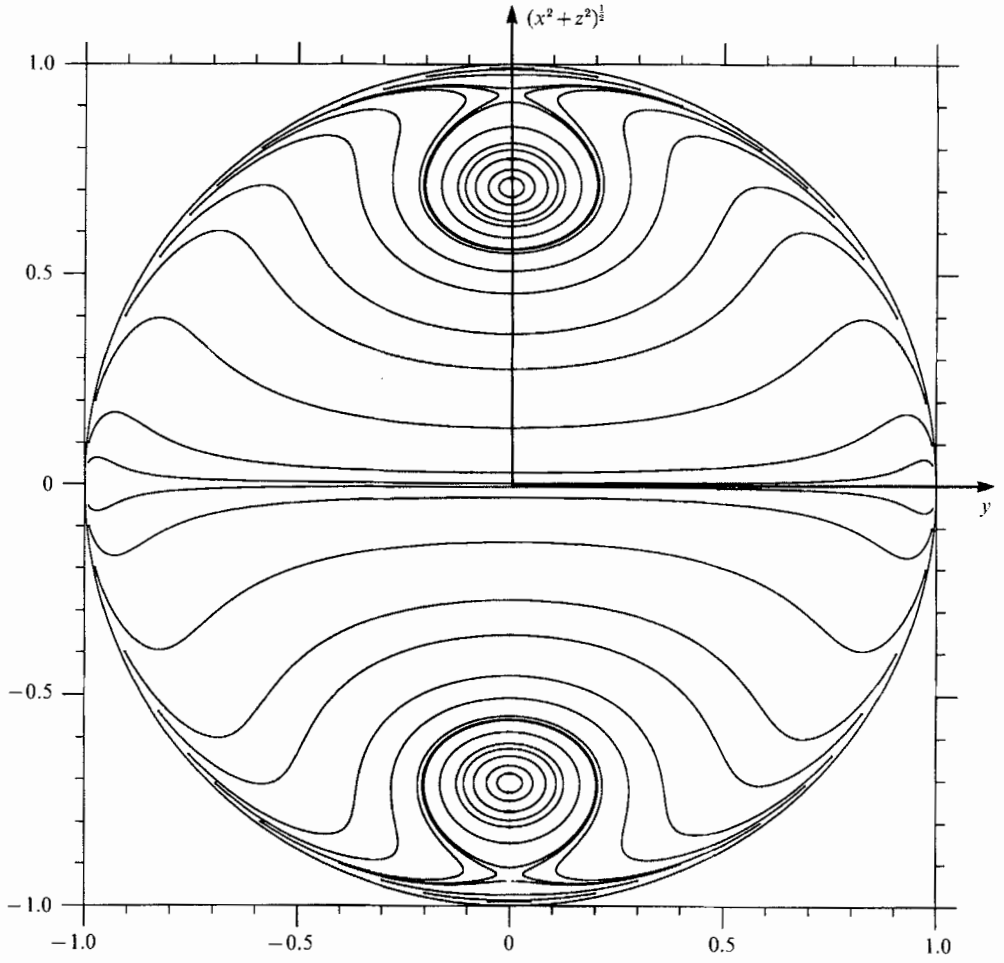

FIGURE 10. Intersection of adiabatic invariant surfaces of the system (7.16) with the plane of section $x = z$.

we find the second invariant†

$$J = (r^2-1)/z^3. \tag{7.14}$$

The integral curves of (7.11) are thus given by the intersections of the surfaces $I =$ const. $J =$ const. Taking z as a parameter on these curves, x and r are given by

$$x = I/z^4, \quad r^2-1 = z^3 J. \tag{7.15}$$

Now, under perturbation of the flow (7.11) by the parameter $\alpha(=\epsilon)$, we find that

$$\left.\begin{aligned} \frac{\mathrm{d}I}{\mathrm{d}t} &= \epsilon z^3(z^2-4x^2) = \epsilon\left(z^5-\frac{4I^2}{z^5}\right), \\ \frac{\mathrm{d}J}{\mathrm{d}t} &= \frac{3\epsilon x(r^2-1)}{z^4} = \frac{3\epsilon IJ}{z^5}, \end{aligned}\right\} \tag{7.16}$$

† Actually, this invariant was found (Bajer 1989) by first casting the equations in canonical Hamiltonian form, with

$$p = y^2 z, \quad q = x, \quad t = z \quad \text{and} \quad H(p,q,t) = -q\left(\frac{4p}{t}+\frac{11}{3}q^2+t^2-3\right).$$

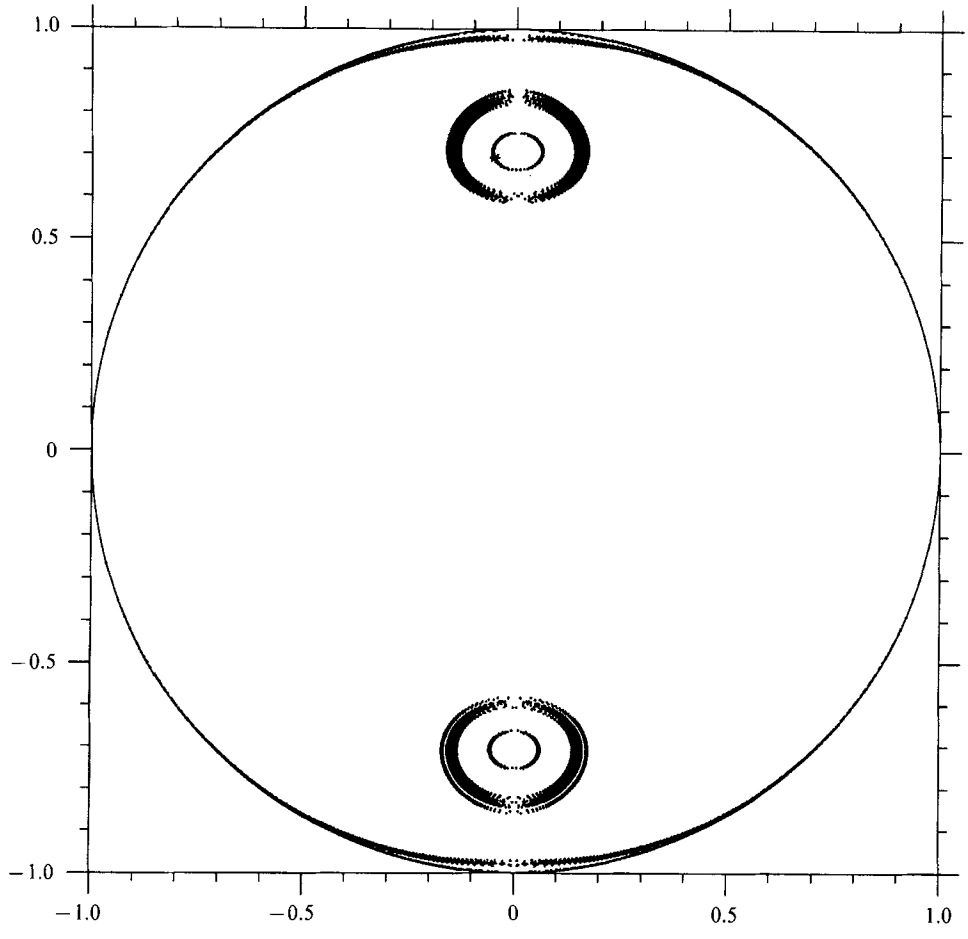

FIGURE 11. Poincaré sections (plane $x = z$) of three trajectories (streamlines) of the flow (1.7) when $\alpha(=\epsilon) = 0.01$ and $\beta = 0$. Each section consists of two parts, one close to the unit circle and the other a pair of small nearly circular bands in the interior (compare figure 10).

so that the adiabatic invariants are given by integrating the system (6.6) with

$$\left.\begin{aligned} \bar{F}(I,J) &= \langle z^5\rangle - 4I^2\langle z^{-5}\rangle, \\ \bar{G}(I,J) &= 3IJ\langle z^{-5}\rangle \end{aligned}\right\} \tag{7.17}$$

where $\langle \dots \rangle$ represents an average over a closed orbit (7.15) labelled by (I,J) (cf. 6.5). Since $\varphi = \omega(I,J)t$ (when $\epsilon = 0$, see (6.4)), these are in effect time-averages on the orbit, e.g.

$$\langle z^5\rangle = \frac{\oint z^5\,\mathrm{d}t}{\oint \mathrm{d}t} = \frac{\int_{z_{\min}}^{z_{\max}} (z^5/2yz)\,\mathrm{d}z}{\int_{z_{\min}}^{z_{\max}} (1/2yz)\,\mathrm{d}z}. \tag{7.18}$$

Evaluation of such integrals requires first determination for each (I,J) of the minimum and maximum values of z on the orbit, then numerical integration. When $\bar{F}(I,J)$, $\bar{G}(I,J)$ are thus determined, the integral curves of (6.6) may be computed. Details of this procedure are given in Bajer (1989). The resulting family of adiabatic

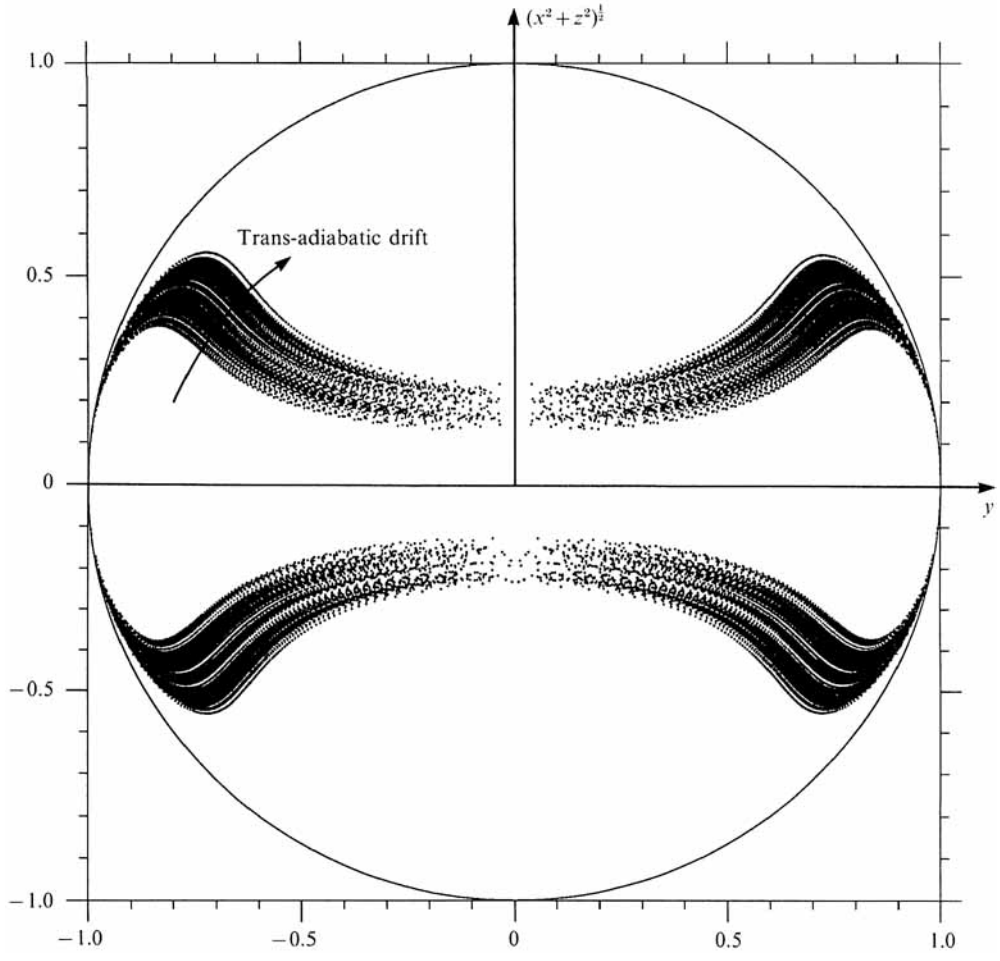

FIGURE 12. Poincaré section (plane $x = z$) for a single trajectory of the STF flow with $\alpha = 0.01$, $\beta = 0$. The trajectory migrates across the family of adiabatic surfaces (compare figure 10), this 'trans-adiabatic drift' occurring while the fluid particle passes near either side of the saddle points at $y = \pm 1$.

surfaces $A(I, J) = \text{const.}$ intersects the plane of section $x = z$ in the family of curves shown in figure 10.

We compare these surfaces with the computed Poincaré sections of the flow for $\beta = 0$ and $\alpha(= \epsilon) = 0.01$ – see figure 11. Sections of three orbits are shown, each consisting of two parts: one close to the unit circle and the other a small circular band in the interior. This feature is evident also in figure 10.

Figure 12 shows another single orbit of (6.3) with an extended integration giving 38500 points of section. The fine structure in this figure faithfully reflects the family of adiabatic curves; but what is most remarkable is the manner in which the solution trajectory can migrate from one adiabatic surface to another, this migration occurring during the relatively long time that a fluid particle spends in neighbourhoods of the (saddle-type) stagnation points at $y = \pm 1$. However weak the rotation may be, the timescale of the unperturbed flow in a sufficiently small neighbourhood of the stagnation points is of the same order in $1/\epsilon$ as the timescale of the perturbation. When the timescales cannot be separated the averaging procedure leading to the equations (6.6) breaks down.

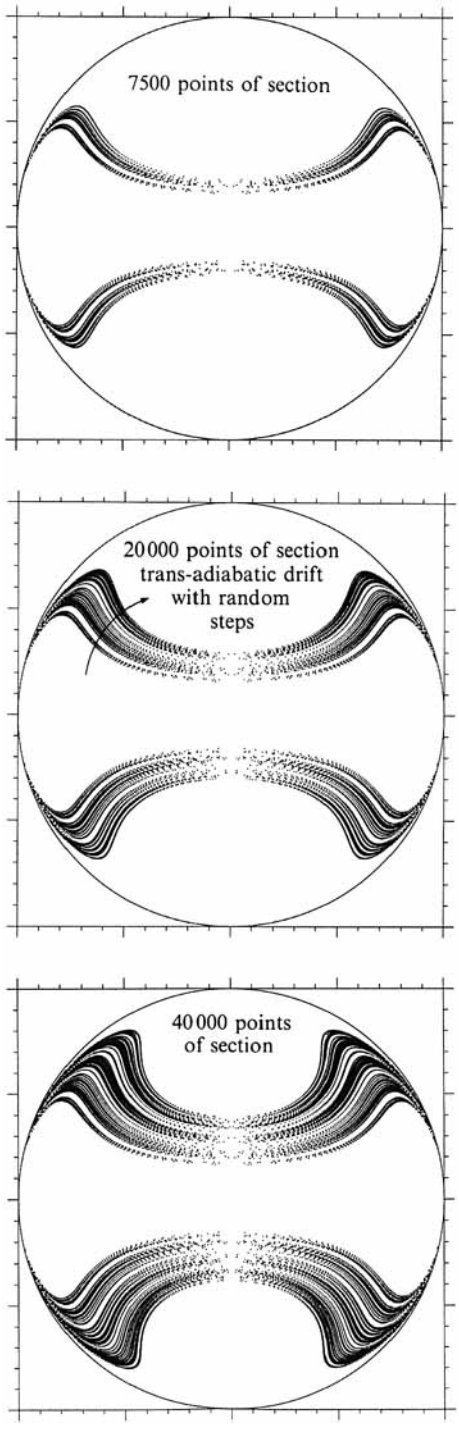

FIGURE 13. Development of Poincaré section for a single trajectory as the number of points of section increases; $\alpha = 0.01$, $\beta = 1$. Note the 'trans-adiabatic drift' with apparently random steps from one adiabatic surface to another (compare figure 10).

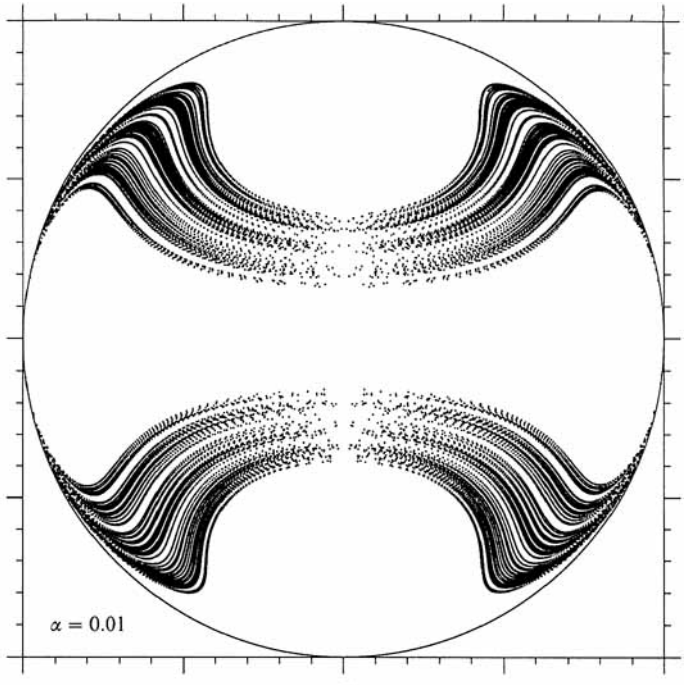

(a)

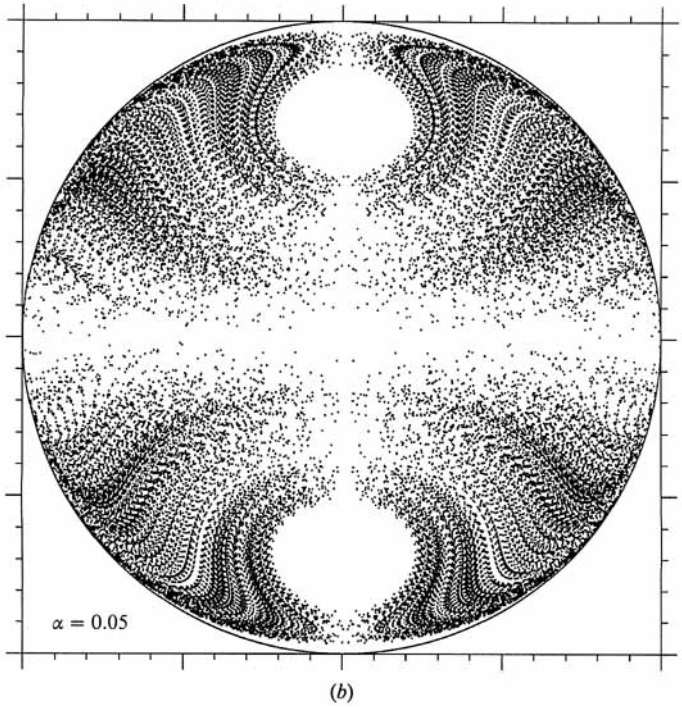

(b)

FIGURE 14(a,b). For caption see p. 361.

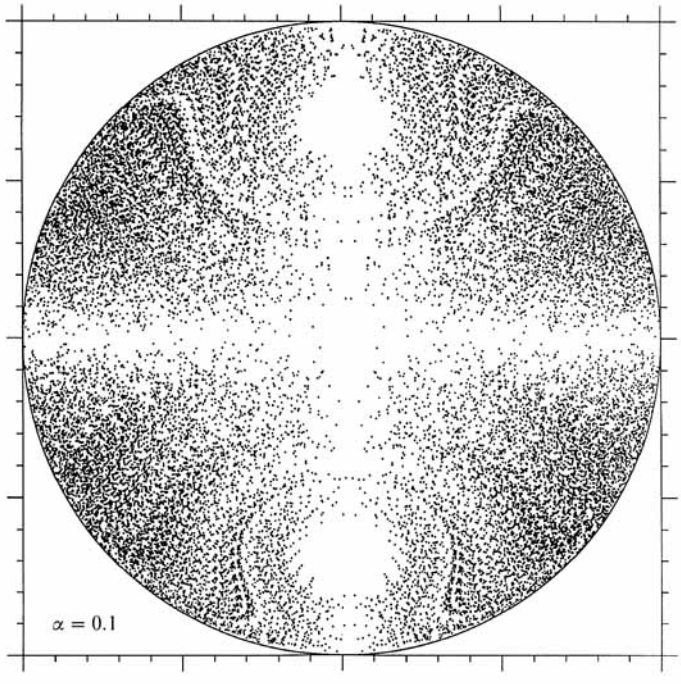

(*c*)

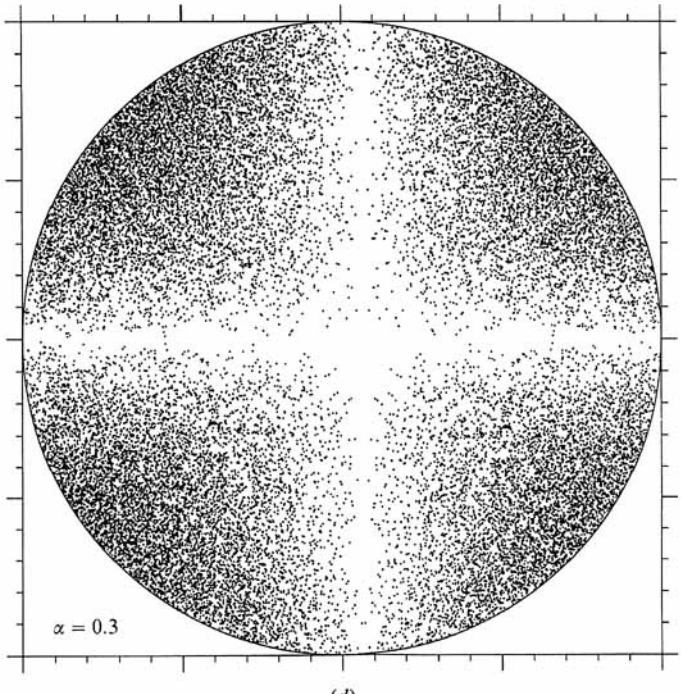

(*d*)

FIGURE 14(*c*,*d*). For caption see p. 361.

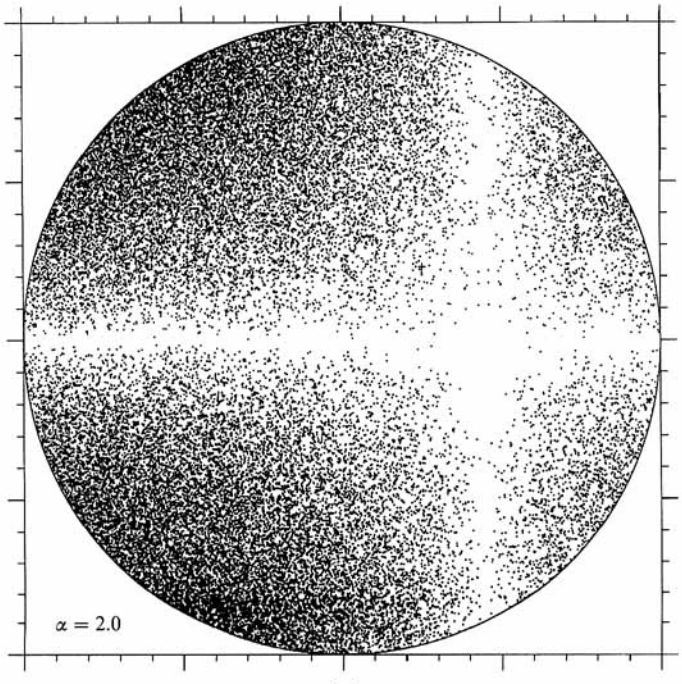

(e)

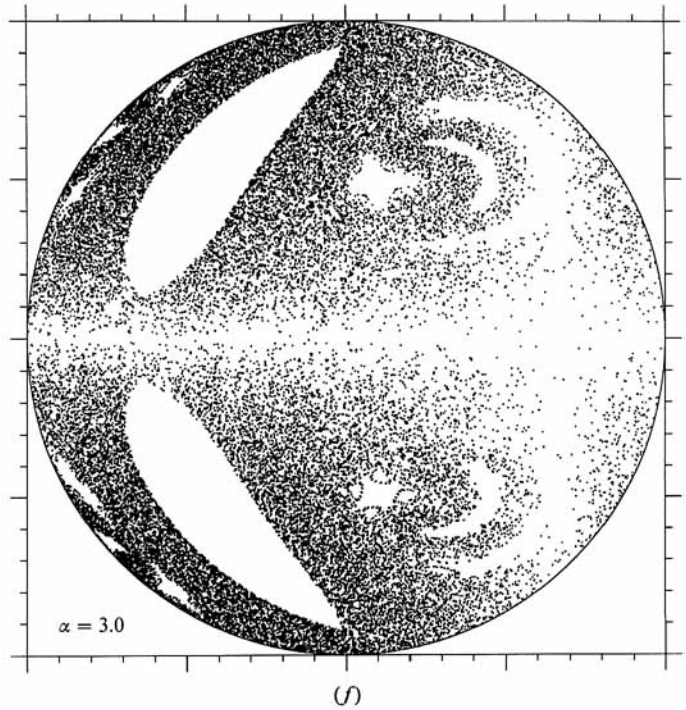

(f)

FIGURE 14(e,f). For caption see p. 361.

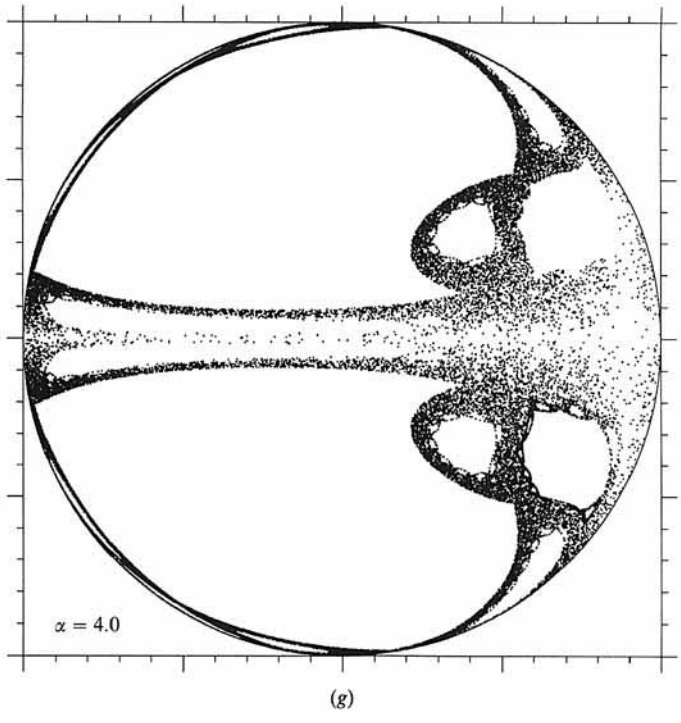

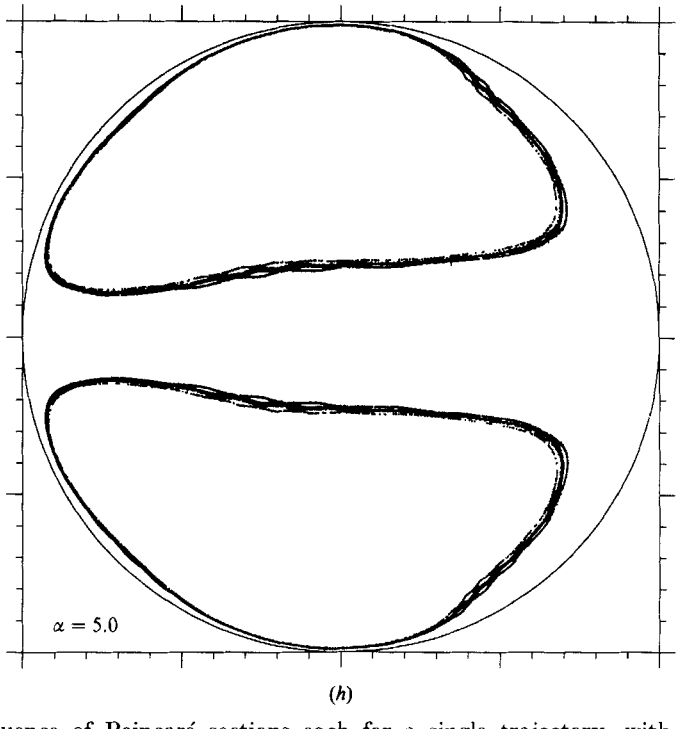

FIGURE 14. Sequence of Poincaré sections each for a single trajectory, with $\beta = 1$ and α as indicated. The sequence shows the transition from the $\alpha \ll 1$ asymptotic behaviour to the $\alpha \gg 1$ asymptotic behaviour.

Owing to the weak rotation about the y-axis, every particle eventually crosses the invariant plane on which particles are rapidly swept towards one of these points and then the jump to a new adiabatic surface occurs. It is this phenomenon that we describe as *trans-adiabatic drift*.† The development of a Poincaré section as the number of points of section increases (figure 13 in this case for $\beta = 1$) shows the progress of this trans-adiabatic drift over a long time-integration.

7.3. *Poincaré sections for* $\beta = 1$ *and* $0 < \alpha < \infty$

Figure 14 shows an extended sequence of Poincaré sections for the case $\beta = 1$ and for $\alpha = 0.01, 0.05, 0.1, 0.3, 2, 3, 4, 5$, with in each case a number of the order of 40000 points of section being plotted. In this sequence we observe the transition from the behaviour identified above for $\alpha \ll 1$ towards that identified for $\alpha \gg 1$. In both limits, the adiabatic invariants provide a vital clue to the structure of the flow. When α is small, trans-adiabatic drift occurs because of the characteristic topology of the unperturbed flow, whereas when α is large, orbits really are constrained to narrow layers of chaos trapped between KAM tori.

When $\alpha = 0.3$, the adiabatic structure is not apparent from the Poincaré section, but it can still be observed in the time-dependent evolution of that section on the monitor screen, as integration proceeds. This suggests that time correlations might reveal this structure, a possibility that we have not as yet pursued.

When α increases to 2, the adiabatic structure is no longer observed, even in the time-dependent evolution of the chaotic structure; with a further increase in α, islands of regularity appear in the sea of chaos. For $\alpha = 4$ these are already a dominant feature, and for $\alpha = 5$, the structure characteristic of the $\alpha \gg 1$ limit (figure 9) is clearly revealed. (We note that the stagnation points at $y = \pm 1$ of the surface flow change from saddle to stable node as α increases through 3.5 and 4.5 respectively.)

8. Conclusions

We have shown that the general quadratic flow in a sphere can be decomposed into a poloidal part of Hill's vortex structure and a toroidal part consisting of a quasi-rigid rotation and a twist ingredient characterized by two positive parameters (the principal rates of twist) λ and ν. The general quadratic flow is non-integrable, but can be expressed as the sum of two integrable flows which provide a basis for analysis by a technique involving adiabatic invariants associated with the perturbation of either flow. These adiabatic invariants define a family of surfaces within the sphere on which particle trajectories remain for a long time. However, we have identified a mechanism whereby particles may migrate from one adiabatic surface to another whenever the unperturbed flow has an invariant plane on which the streamlines are 'quasi-parabolic' in character. The condition for this is essentially that the twist ingredient of the undisturbed flow should dominate over the poloidal ingredient ($a_2^2 < \lambda\nu$ in the notation of §5).

The stretch–twist–fold (STF) flow (1.7), motivated by earlier dynamo-theory studies, is a superposition of two flows, one of which satisfies the above condition, and it has been subjected to detailed analysis and numerical experiment. A range of

† In a preliminary account of this work (Bajer, Moffatt & Nex 1990) we used the term 'super-adiabatic'. This term is sometimes used, in a different context, to describe invariants which are conserved to higher order than normal adiabatic invariants (M. Berry private communication; Lichtenberg & Lieberman 1983, p. 458). We therefore use the term 'trans-adiabatic' here to avoid config

behaviour is revealed which can be well understood in terms of the adiabatic invariants when the parameter α of the flow is either large or small. The topology of the adiabatic surfaces has an important influence on the behaviour: when α is large, these are nested tori, while when α is small, they all meet at stagnation points of the flow, so the behaviour is very different in these two cases. For values of α in the range 1–2, the streamlines are apparently completely chaotic within the sphere. This type of phenomenon is now well known for certain *unsteady* Stokes flows in two-dimensions (Chaiken *et al.* 1986) but we believe that this is the first explicit example of a steady Stokes flow in a bounded region exhibiting chaotic streamlines.

It is evident that the quadratic term of the Taylor expansion (1.1) encapsulates a remarkable richness of structure, which perhaps merits more attention in this purely fluid-mechanical context than it has hitherto received.

This paper is dedicated to George Batchelor who has been an inspiration and a guide to both of us over many years and in many different ways.

One of us (K.B.) has been supported in the course of this research by a Research Studentship at Trinity College, Cambridge, and by a Research Contract, no. EMR 470M, with Culham Laboratory, UKAEA.

REFERENCES

AREF, H. 1984 Stirring by chaotic advection. *J. Fluid Mech.* **143**, 1–21.

AREF, H. & BALACHANDAR, S. 1986 Chaotic advection in a Stokes flow. *Phys. Fluids* **29**, 3515–3521.

ARNOL'D, V. I. 1973 *Ordinary Differential Equations*. MIT Press.

ARNOL'D, V. I. 1978 *Mathematical Methods of Classical Mechanics*. Springer.

BAJER, K. 1989 Flow kinematics and magnetic equilibria. Ph.D. thesis, Cambridge University.

BAJER, K., MOFFATT, H. K. & NEX, F. 1990 Steady confined Stokes follows with chaotic streamlines. In *Topological Fluid Mechanics, Proc. IUTAM Symp.* (ed. H. K. Moffatt & A. Tsinober). Cambridge University Press.

BATCHELOR, G. K. 1967 *An Introduction to Fluid Dynamics*. Cambridge University Press.

CHAIKEN, J., CHEVRAY, R., TABOR, M. & TAN, Q. M. 1986 Experimental study of Lagrangian turbulence in a Stokes flow. *Proc. R. Soc. Lond.* A**408**, 165–174.

CHAIKEN, J., CHU, C. K., TABOR, M. & TAN, Q. M. 1987 Lagrangian turbulence and spatial complexity in Stokes flow. *Phys. Fluids* **30**, 687–694.

DOMBRE, T., FRISCH, U., GREENE, J. M., HÉNON, M., MEHR, A. & SOWARD, A. M. 1986 Chaotic streamlines in the ABC flows. *J. Fluid Mech.* **167**, 353–391.

HÉNON, M. 1966 Sur la topologie des lignes de courant dans un cas particulier. *C.R. Acad. Sci. Paris* **262**, 312–314.

LICHTENBERG, A. J. & LIEBERMAN, M. A. 1983 *Regular and Stochastic Motion*. Applied Mathematical Sciences, vol. 38. Springer.

MOFFATT, H. K. 1969 The degree of knottedness of tangled vortex lines. *J. Fluid Mech.* **35**, 117–129.

MOFFATT, H. K. 1978 *Magnetic Field Generation in Electrically Conducting Fluids*. Cambridge University Press.

MOFFATT, H. K. & PROCTOR, M. R. E. 1985 Topological constraints associated with fast dynamo action. *J. Fluid Mech.* **154**, 493–507.

VAINSHTEIN, S. I. & ZEL'DOVICH, YA. B. 1972 Origin of magnetic fields in astrophysics. *Sov. Phys. Usp.* **15**, 159–172.

ZEL'DOVICH, YA. B., RUZMAIKIN, A. A. & SOKOLOV, D. D. 1983 *Magnetic Fields in Astrophysics*. Gordon & Breach.